Articles

Methanol Oxidation Effect on Carbon Supported Pt Particles Studied by ^{13}C NMR, XRD, and TEM

Kee Sung Han and Oc Hee Han*

*Analytical Research Division, Daegu Center, Korea Basic Science Institute, Daegu 702-701, Korea. *E-mail: ohhan@kbsi.re.kr*

Received March 23, 2006

Methanol oxidation effect on carbon supported Pt was investigated as a function of Pt content in a sample which is closely correlated with Pt particle sizes. After prolonged methanol oxidation the Pt particle size did not change within the experimental error ranges. The ^{13}C chemical shift and linewidth of CO adsorbed on Pt show non-linear behavior simply due to the Pt particle size difference. The Pt size variation difference between this work and the previous reports of the particle growths is explained by the experimental temperature difference.

Key Words : Methanol oxidation, Pt particle size, Pt supported on carbon, ^{13}C NMR, TEM

Introduction

Platinum and its alloys such as Pt-Ru supported on high surface area carbon[1] have attracted great scientific attention as important heterogeneous catalyst for fuel cells[2] like direct methanol fuel cell (DMFC)[3] due to its high reactivity. Unfortunately, such high reactivity can make it difficult to investigate the properties of highly dispersed metal catalysts because the properties depend strongly on the particle size and surface morphology which can be easily influenced by sample preparation procedures,[4-6] pretreatment such as cleaning,[7,8] and the properties of supporting materials.[9,10] In fact, the particle size and surface morphology of Pt are influenced by electrochemical potentials.[11,12] The surface morphology of metals are also changed by oxidation of hydrogen or reduction of oxides and oscillated by oxidation and reduction cycles in oxide supported metals.[13-15]

CO poisoning occurring during methanol oxidation is one of the major problems to overcome in real DMFC operation. It can influence the structure and morphology of the Pt particles of catalysts and hence the catalytic activity. There have been many research reports on CO induced surface variations such as surface reconstruction,[16,17] surface lifting,[18,19] sites switching,[20] and structure transformation[21,22] in model catalysts.

The Pt/C catalysts of proton exchange membrane fuel cell in real cell operation were known to cause Pt particle growth and agglomeration along the operation time.[23,24] In contrast, not only Pt particle growth was observed in phosphoric acid fuel cells during cell operation condition[11] but also corrosion of carbon supports and dissolution of Pt in open circuit voltage condition[25] due to higher operation temperature and stronger acidic condition. In general particle sizes and surface morphology of Pt particles are known to be easily influenced by thermal treatment even not under any cell operation condition.[1,11] However, the structural variation of Pt particles by prolonged methanol oxidation in the real commercial catalysts at room temperature, which can separate the temperature and methanol oxidation effect, is not reported yet as far as we know. Therefore, not only for fundamental electrochemistry research but also for efficient application, it is essential to understand what occurs in the commercial catalysts by successive poisoning and removing it during methanol oxidation under electrochemical environments. In this work, we characterize Pt particle property variations in carbon supported Pt catalysts due to prolonged methanol oxidation by means of ^{13}C nuclear magnetic resonance (NMR), X-ray diffraction (XRD), and transmission electron microscopy (TEM) primarily.

XRD[4,5,12,23,24,26,27] and TEM[4-8,11,24,27] have been widely used in determining the Pt particle sizes of catalysts while NMR has been proved useful in deducing the electronic properties of metals and heterogeneous catalysts.[28-30] Especially, NMRE (NMR+electrochemistry) method was useful to study electrochemical heterogeneous catalysts.[31-33] In this work ^{13}C NMR of CO adsorbed on Pt surface by partial oxidation of ^{13}C enriched methanol was employed to compare the Pt supported on carbon samples because it is more sensitive compared to ^{195}Pt NMR in probing the surface conditions of Pt nanoparticles before and after methanol oxidation. In addition, CO stripping cyclic voltammetry (CV) was performed to check catalytic activity variations of the samples.[8]

Experimental Section

Sample preparation. Carbon supported Pt (X = 20, 40 and 60% supported on Vulcan XC-72, E-Tek Inc., USA) samples were purchased. The purchased X% Pt/C samples of about 400-500 mg without mixing with any filler were directly loaded[34] onto the Pt boat working electrode made of a 25×25 mm size Pt foil immersed in 0.5 M H_2SO_4

electrolyte solution first and then cleaned by holding the cell potential at 250 mV (*vs*. 1 M Ag|AgCl reference) until the reduction current was decreased to less than –200 μA.[7,8,33] All the samples in this work were cleaned by this 'holding the potential at 250 mV' first.

All potentials were controlled by a model 362 Scanning Potentiostat (EG & G, USA) and measured versus 1 M Ag|AgCl electrode. 99.9% ^{13}C enriched methanol (Cambridge Isotope Laboratories Inc., U.S.A) and 96% suprapure sulfuric acid (Merck, Germany) were used to prepare 0.6 M $^{13}CH_3OH$ and 0.5 M H_2SO_4 solution. For natural isotope 0.6 M CH_3OH and 0.5 M H_2SO_4 solution, ChromAR® HPLC grade CH_3OH (Mallinckrodt Baker Inc., Paris, Kentucky, U.S.A.) was used. To prevent oxygen penetration into the electrolyte solution and the electrochemical cell, ultra pure Ar gas (99.999%, Hankuk Sanup Gas Ltd., Korea) which is moisture-saturated by passing through water, was purged into the electrolyte solution in the flask.

Holding-at-250mV-X samples: ^{13}CO was adsorbed onto catalysts cleaned at 250 mV as described above by partial oxidation of about 30 mL ^{13}C enriched methanol solution (0.6 M $^{13}CH_3OH$/0.5 M H_2SO_4)[35,36] at the potential of 0 mV until the current was reduced below +200 μA. These samples are denoted as 'holding-at-250mV-X', where X = 20, 40 and 60.

R-CO-X samples: The samples were prepared by cleaning first and then successively adsorbing CO on the loaded samples of ~500 mg in 30 mL 0.6 M CH_3OH/0.5 M H_2SO_4 solution at 0 mV for about 100 hours until the current was dropped below +200 μA. Then the potential was changed to 450 mV for oxidation of methanol in solution as well as of CO adsorbed at 0 mV, which completes the prolonged methanol oxidation. Finally, when the current was reduced below +200 μA, ^{13}CO for ^{13}C NMR detection was adsorbed at 0 mV by partial oxidation of $^{13}CH_3OH$ in freshly replaced 0.6 M $^{13}CH_3OH$/0.5 M H_2SO_4 solution.

R-^{13}CO-X samples: The samples were prepared by the same procedure for 'R-CO-X' samples except the fact that 0.6 M $^{13}CH_3OH$/0.5 M H_2SO_4 solution, instead of 0.6 M CH_3OH/0.5 M H_2SO_4 solution, was initially used during the prolonged methanol oxidation.

R2-CO-60 samples: The samples were prepared with 60% Pt/C by repeating the prolonged methanol oxidation twice by replacing the 0.6 M CH_3OH/0.5 M H_2SO_4 solution in the cell with another fresh 0.6 M CH_3OH/0.5 M H_2SO_4 solution after the current at 450 mV was reduced below +200 μA. The other sample preparation procedures are the same with those for R-CO-X samples.

R-CO-20-p samples: The samples were made by the same preparation procedure for R-CO-20 or R-^{13}CO-20 samples except the fact that 0.5 M H_2SO_4 solution without methanol in it, instead of 0.6 M $^{13}CH_3OH$/0.5 M H_2SO_4 or 0.6 M CH_3OH/0.5 M H_2SO_4 solution was used in the prolonged methanol oxidation step. Since there is no methanol to react in 0.5 M H_2SO_4 solution, the effect of the electrochemical potentials applied during the prolonged methanol oxidation can be checked by comparing R-CO-20 or R-^{13}CO-20 samples with this sample.

Sealing the NMR samples. For ^{13}C NMR experiment, the samples prepared as described above were rinsed with 0.5 M H_2SO_4 solution to remove excess methanol, if any, and then transferred to a specially made NMR tube.[36] The sample tube was sealed after purging several times with Ar gas.

Characterization. TEM and XRD data were acquired with H-7100 at 100 kV (Hitachi, Japan) and X'Pert PRO-MPD (PANanalytical, Netherlands), respectively.

The ^{13}C NMR experiments were carried out with a 600 MHz Unity INOVA spectrometer (Varian Inc., USA) using a home-made probe. ^{13}C NMR spectra were acquired by using a Hahn echo pulse sequence ($\pi/2 - \tau_0 - \pi - \tau_1$ – echo acquisition with τ_0 = 20 μs and τ_1 = 13 μs) at ambient temperature. The spectrum was constructed point-by-point[37] from spin echo signals obtained at different radio frequencies with a 5 kHz interval. The $\pi/2$ pulse length, 22 μs, was measured with the ^{13}CO adsorbed on carbon supported Pt samples while the chemical shift was calibrated with neat tetramethylsilane (TMS) as an external reference sample. The CO stripping CV between –230 and 700 mV at 0.2 mV/s scanning speed was obtained from 40-60 mg Pt catalysts remained in the Pt boat after NMR sample preparation. Further details of all these experiments can be found elsewhere.[7,8]

Results and Discussion

Pt particle sizes were determined by TEM and XRD and the average particle sizes measured are summarized in Table 1. An average length of each coherent domain is calculated from the powder XRD line broadening of corresponding Bragg reflections using Scherrer-type equation after correction for instrumental broadening.[26,27] Our XRD result has inherent error in measuring particle size because it measures rather crystallite size than particle size and the carbon support contributes background signals. The crystallite size and particle size are synonymous in very small particles, about up to ~5 nm size.[27] The linewidths are wider as the

Table 1. The average particle size (nm) from TEM and XRD

	20% Pt/C		40% Pt/C		60% Pt/C	
	TEM	XRD	TEM	XRD	TEM	XRD
Holding-at-250 mV	2.7 ± 1.1	2.8 ± 0.3	4.7 ± 1.2	4.6 ± 0.3	6.1 ± 2.0	5.5 ± 0.3
R-^{13}CO	3.1 ± 1.0	2.7 ± 0.3	5.1 ± 1.0	4.3 ± 0.3	6.3 ± 2.2	5.9 ± 0.3
R-CO	3.5 ± 1.0	3.0 ± 0.3	4.7 ± 1.2	4.3 ± 0.4	5.1 ± 1.4	5.8 ± 0.3

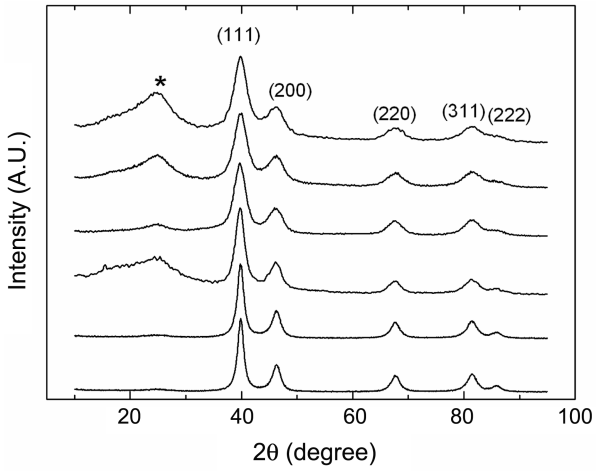

Figure 1. Powder XRD patterns of holding-at-250mV-20, R-CO-20, holding-at-250mV-40, R-CO-40, holding-at-250mV-60 and R-CO-60 sample from top to bottom. Miller index of each diffraction signal is denoted on the top of the signal and broad carbon background signal is marked by *.

domain lengths are smaller and the domain lengths of different Bragg reflections for a particle are similar to one another as particle shapes are closer to spheres.[27] For our calculation of domain lengths, 5 peaks at 2θ = 39.7, 46.2, 67.5, 81.3 and 85.7° marked in Figure 1 are used and the lengths calculated were the same within the error range. The average of the five domain lengths is presented in Table 1. Although carbon supported Pt particles such as in our samples are typically single crystallites, some Pt particles tend to aggregate during some pretreatment, especially in the samples of high dispersion and high Pt loading. At the same time, XRD would not observe well, if any, less-ordered particles (close to amorphous state) or crystalline particles but too small to be detected by XRD. In addition, in measuring bigger particle sizes, XRD and TEM data inherently have smaller and larger error, respectively, since line broadening in XRD and particle lengths in TEM is narrower and longer, respectively. TEM also has a weak point to see only a small portion of the sample although this weak point can be mitigated somewhat by taking many TEM data for a sample. TEM data can provide not only average particle sizes but also particle size distributions as shown in Figure 2. Although the absolute particle length measured by XRD and TEM can be different, the data trends are expected to be consistent. However, after the prolonged methanol oxidation, in Table 1, all the particle size data can be interpreted as the same within the experimental errors. Overall discrepancies in the particle size trend are observed between XRD and TEM data and the 60% Pt/C samples show worst scattering and discrepancy between TEM (~7% decrease) and XRD data (~5% increase). To confirm the particle size variation trends by the third method, relative Pt surface area changes due to the prolonged methanol oxidation were calculated from the peak areas in ^{13}C NMR spectra and the CO coverage (θ_{CO}/$2\theta_H$) data obtained from a CO stripping CV as presented in Figure 3. The carbon black signal in the ^{13}C NMR spectra is

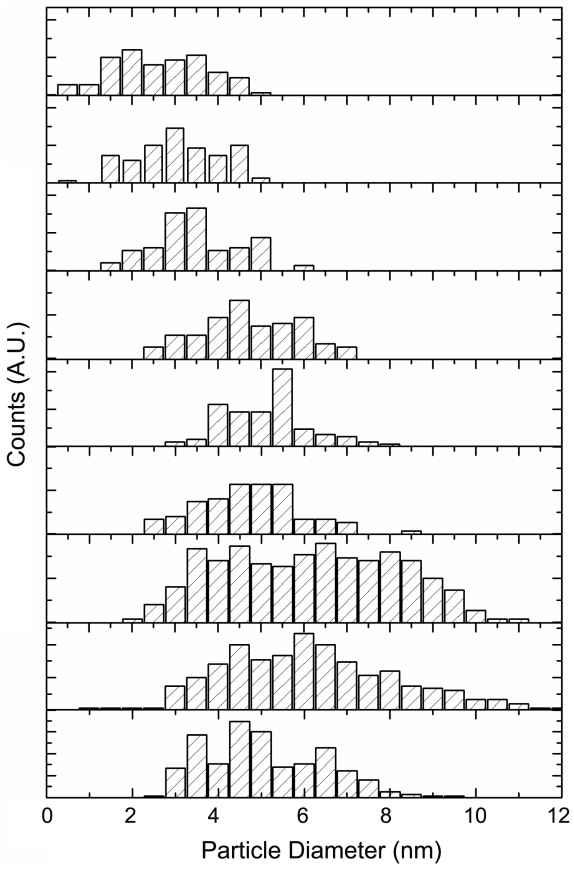

Figure 2. Histograms of particle sizes obtained from TEM images of holding-at-250mV-20, R-^{13}CO-20, R-CO-20, holding-at-250mV-40, R-^{13}CO-40, R-CO-40, holding-at-250mV-60, R-^{13}CO-60, and R-CO-60 sample from top to bottom.

about 1% of the total carbon numbers in a sample since ^{13}C is 1% in natural abundance while all CO on Pt contributes to the CO signal since CO was enriched with ^{13}C to 99.9%. For the Pt/C samples of a certain Pt weight percentage, CO signals are proportional to the CO coverage and the Pt surface areas when the carbon black signals are set to an equal area. From this relationship, surface areas of Pt can be monitored before and after methanol oxidation. The surface area of Pt was changed to 73 ± 14, 107 ± 20, and 84 ± 20% for 20, 40, and 60% Pt/C samples, respectively. From these data, we can conclude that the average Pt particle size increased in 20% and did not change in 40% and 60% Pt/C samples. However, even for 20% Pt/C samples it is hard to conclude any Pt size change by the methanol oxidation if all the Pt size measurement data are considered.

To test the oxidation time dependence, a 60% Pt/C sample, R2-CO-60, was made with repeating the prolonged methanol oxidation procedure twice. However, Pt particle sizes of R2-CO-60 were the same with those of R-CO-60 within the error ranges in terms of average size and particle size distribution pattern. In addition, the possibility was checked with R-^{13}CO-20-p samples whether the particle size variations are due to applied electrochemical potentials[11] during the prolonged methanol oxidation rather than the methanol

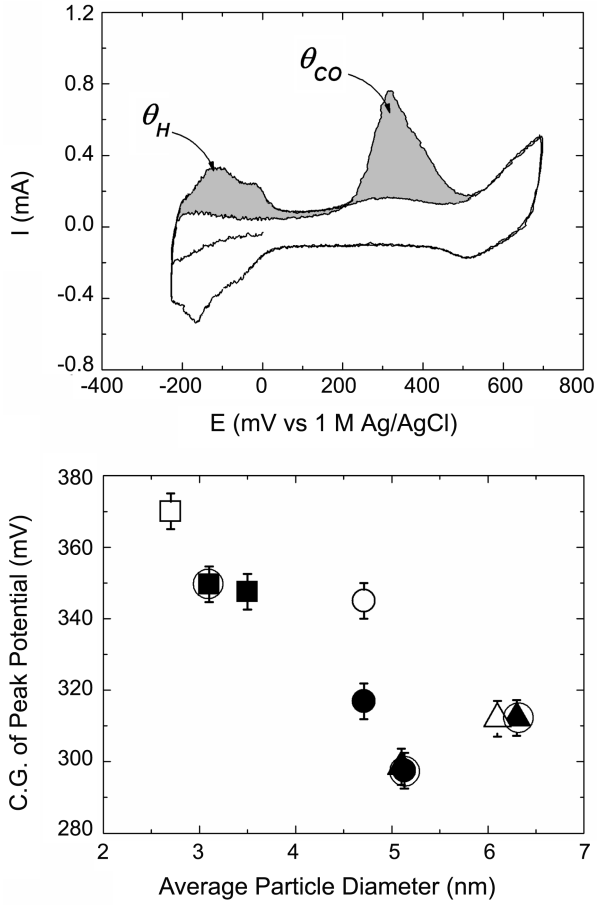

Figure 3. The CO stripping CV of a holding-at-250mV-20 sample (top) and a plot of center of gravity of CO oxidation peak potential of CO stripping CV versus average Pt particle size measured by TEM (bottom). Square, circle, and triangle shapes represent 20, 40, and 60% Pt/C sample data, respectively. Filled shapes are used for R-CO-X data whereas additional outer circle is added to the filled shape to denote R-^{13}CO-X data.

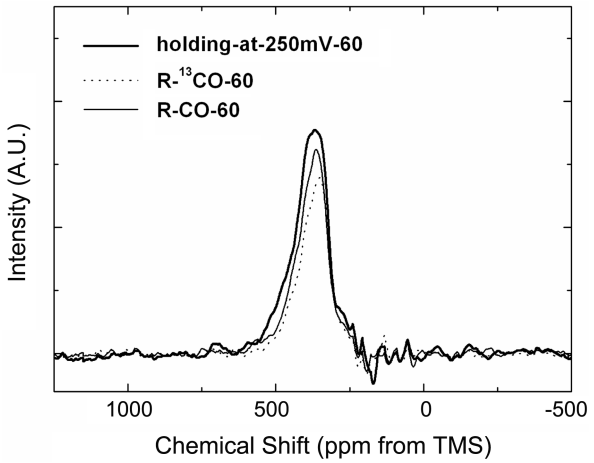

Figure 4. The ^{13}C NMR spectra of adsorbed ^{13}CO on 60% Pt supported on carbon samples after subtracting the carbon graphite signal.

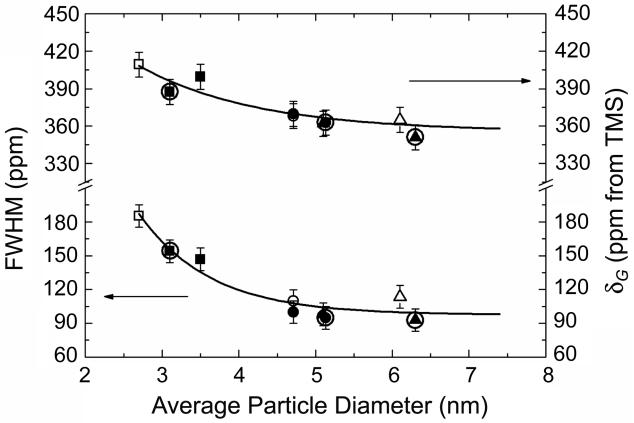

Figure 5. The full width at half height (FWHM) and the center of gravity (δ_G) plot of the ^{13}CO NMR spectra with respect to average particle size taken from our TEM results: Square, circle, and triangle shapes represent 20, 40, and 60% Pt/C sample data, respectively. Filled shapes are used for R-CO-X data whereas additional outer circle is added to the filled shape to denote R-^{13}CO-X data.

oxidation reaction itself. The samples did not provide any evidence of Pt particle size change by the applied potentials.

Nanostructural difference of initial Pt particles can bring difference of particle size change by methanol oxidation. Nevertheless, there were no difference of nanostructures between our samples and the samples we compared with[11,23,24] or between our samples with different Pt loading. Then the main factor for the difference between our observation and the previous reports on Pt growth would be the reaction temperatures. All our reactions were carried out at room temperature while temperatures higher than room temperature were employed in the previous reports. Pt particles were known to grow at high temperature[1,11,38] even without any cell operation. Therefore, it is more likely that methanol oxidation itself does not induce metal particle growth but high temperature effect and/or synergic influence of the oxidation reaction and high temperature are present at such high cell operating temperatures.

The plot in Figure 3 shows the center of gravity of CO stripping peak potential, inversely proportional to electrocatalytic activity,[35] decreases as average Pt particle size increases. This is consistent with the previous result[8] and that CO oxidation reaction is structure sensitive and more active on face sites.[38]

Figure 4 shows representative ^{13}C NMR spectra of ^{13}CO adsorbed on the Pt surfaces of the Pt supported on carbon samples. These peaks are closely related to the electronic states of surface Pt.[39] The peak intensities of ^{13}CO on Pt are proportional to the Pt surface areas and CO coverage of each sample. The linewidth (full width at half maximum; FWHM) and the center of gravity (δ_G) of the CO peaks, determined after subtracting carbon black signal, are plotted in Figure 5. In general, the linewidths are known to be narrower for the larger Pt particles[36] and not to vary much for Pt particles larger than about 5 nm.[8] Likewise, δ_G decreases and then becomes steady as the Pt particle size grows. As a result, our plots of δ_G and linewidth are insensitive to whether they are plotted versus the particle size measured either by XRD or

TEM. From the steeper change of both the linewidth and δ_G of Pt/C for the Pt size smaller than 5 nm could be interpreted by different relative population of various surface adsorption sites of Pt particles versus the Pt particle size as explained previously.[8]

CO coverage of our samples was also checked due to controversy of its Pt particle size dependence.[36,40] Fermi level local density of states, which is proportional to δ_G of ^{13}C NMR of CO adsorbed on Pt surfaces,[33,39] was found to be dependent on CO coverage.[41] However, our samples have constant CO coverage of 0.7-0.8 monolayer, which is well in agreement with previous report.[42] Hence our ^{13}C NMR data can be interpreted without considering its CO coverage dependence.

The linewidths for 'R-CO-X' and 'R-^{13}CO-X' samples are the same within the error range. Although δ_G values of 'R-^{13}CO-X' samples are always smaller than those of 'R-CO-X' samples in the same Pt percentage, the differences still remain within the experimental error range. Thus it hardly suggests that the chemical shift of poisoning species produced during the prolonged methanol oxidation is smaller than that of ^{13}CO adsorbed at the last step of the sample preparation for ^{13}C NMR detection. The poisoning species would be labeled by ^{13}C for 'R-^{13}CO-X' but not for 'R-CO-X' samples. Therefore, the linewidth, center of gravity, or intensity of the R-^{13}CO-X sample is expected to differ from that of the corresponding R-CO-X sample if the poisoning species amount is enough to be detected by ^{13}C NMR. However, our results indicate that the poisoning species possibly created by sequential electrochemical reaction of methanol at 0 and 450 mV with the first methanol solution could not be differentiated from ^{13}CO adsorbed at the last step of the sample preparation for ^{13}C NMR detection, possibly due to insufficient amount of the poisoning species for the detection. The detection limit of S/N~2 for ^{13}C NMR for this kind of sample should be typically about 1 molecule per 15 nm^2 on the Pt surface of ~50 m^2 at the field of 14.1 T and at room temperature.[43] Therefore, the poisoning species in our sample must be less than about 0.014 mL, if present any.

Conclusions

By prolonged methanol oxidation process the Pt particle size of Pt/C samples changed negligibly. The ^{13}C NMR results of ^{13}CO on Pt surfaces simply represent the variation of linewidth and chemical shift by the Pt particle size without any additional information such as influence of poisoning species. Probably the number of poisoning species produced is too small to be detected by this ^{13}C NMR method. The Pt size variation behavior difference between this work carried out at room temperature and the previous reports of the particle growths observed as a result of cell operation would be mainly due to experimental temperature difference. Higher temperatures are known to induce sintering of metal particles even without any fuel oxidation reaction. In addition, cell operation can result in synergic influence on the catalysts by methanol oxidation and high temperature. This possible synergic effect and the influence of initial nanoscale structural difference of Pt particles will be worthwhile to study in next step.

Acknowledgement. This work is supported by MOST (Ministry of Science & Technology in Korea) through an International Cooperation Project (Grant M60302000200) and partially by KRCFST (Korea Research Council Fundamental Science and Technology). Authors acknowledge Mr. Sang Geul Lee and Mr. Ki Ju Hwang at the KBSI (Deagu) for taking the XRD and TEM data, respectively. Dr. P. K. Babu at University of Illinois at Urbana-Champaign is greatly acknowledged for his helpful comments.

References

1. Antolini, E. *Mater. Chem. & Phys.* **2003**, *78*, 563.
2. Acres, G. J. K.; Hards, G. A. *Phil. Trans. R. Soc. Lond. A* **1996**, *354*, 1671.
3. Arico, A. S.; Srinivasan, S.; Antonucci, V. *Fuel Cells* **2001**, *1*, 133.
4. Prabhuram, J.; Wang, X.; Hui, C. L.; Hsing, I.-M. *J. Phys. Chem. B* **2003**, *107*, 11057.
5. Teranishi, T.; Hosoe, M.; Tanaka, T.; Miyake, M. *J. Phys. Chem. B* **1999**, *103*, 3818.
6. Frelink, T.; Visscher, W.; van Veen, J. A. R. *J. Electroanal. Chem.* **1995**, *382*, 65.
7. Han, K. S.; Han, O. H. *Electrochim. Acta* **2001**, *47*, 519.
8. Han, K. S.; Han, O. H.; Babu, P. K. *J. Electrochem. Soc.* **2005**, *152*, J131.
9. Stakheev, A. Yu.; Kustov, L. M. *Appl. Catal. A: General* **1999**, *188*, 3.
10. Rodriguez-Reinoso, F. *Carbon* **1998**, *36*, 159.
11. Antolini, E. *J. Mater. Sci.* **2003**, *38*, 2995.
12. Kinoshita, K.; Routsis, K.; Bett, J. A. S. *Electrchim. Acta* **1973**, *18*, 953.
13. Triaca, W. E.; Arvia, A. J. *J. Appl. Electrochem.* **1990**, *20*, 347.
14. Hu, C.-C.; Liu, K.-Y. *Electrochim. Acta* **1999**, *44*, 2727.
15. Surnev, S.; Schoiswohl, J.; Kresse, G.; Ramsey, M. G.; Netzer, F. P. *Phys. Rev. Lett.* **2002**, *89*, 246101.
16. Thostrup, P.; Kruse Vestrgaard, E.; An, T.; Laegsgaard, E.; Besenbacher, F. *J. Chem. Phys.* **2003**, *118*, 3724.
17. Rasko, J. *J. Catal.* **2003**, *217*, 478.
18. van Beurden, P.; Bunnik, B. S.; Kramer, G. J. *Phys. Rev. Lett.* **2003**, *14*, 066106.
19. Baily, C. J.; Surman, M.; Russell, A. E. *Surf. Sci.* **2003**, *523*, 111.
20. Moula, Md. G.; Mishra, A. B. P.; Rzeznicka, I.; Kislyuk, M. U.; Liu, S.; Ohno, Y.; Matsushima, T. *Chem. Phys. Lett.* **2001**, *341*, 225.
21. van Beurden, P.; Kramer, G. J. *J. Chem. Phys.* **2004**, *121*, 2317.
22. Rzeznicka, I.; Moula, Md. G.; de la Garza, L. M.; Ohno, Y.; Matsushima, T. *J. Chem. Phys.* **2003**, *119*, 9829.
23. Cheng, X.; Chen, L.; Peng, C.; Chen, Z.; Zhang, Y.; Fan, Q. *J. Electrochem. Soc.* **2004**, *151*, A48.
24. Wilson, M. S.; Garzon, F. H.; Sickafus, K. E.; Gottesfeld, S. *J. Electrochem. Soc.* **1993**, *140*, 2872.
25. Alderucci, V.; Passalacqua, E.; Giordano, N.; Antonucci, P. L.; Parmigiani, F.; Ricci, N. *J. Appl. Electrochem.* **1990**, *20*, 235.
26. Jenkins, R.; Snyder, R. L. *Introduction to X-ray Powder Diffractometry*; Wiley Interscience: New York, 1996; p 89.
27. Adams, C. R.; Benesi, H. A.; Curtis, R. M.; Meisenheimer, R. G. *J. Catal.* **1962**, *1*, 336.
28. van der Klink, J. J.; Brom, H. B. *Prog. NMR Spectrosc.* **2000**, *36*, 89.

29. van der Klink, J. J. *Adv. Catal.* **2000**, *44*, 1.
30. Fraissard, J. *Catalysis Today* **1999**, *51*, 481.
31. Wu, J.; Day, J. B.; Franaszczuk, K.; Montez, B.; Oldfield, E.; Wieckowski, A.; Vuissoz, P. A.; Ansermet, J. P. *J. Chem. Soc., Faraday Trans.* **1997**, *93*(6), 1017.
32. Babu, P. K.; Tong, Y. Y.; Kim, H. S.; Wieckowski, A. *J. Electroanal. Chem.* **2002**, *524-525*, 157.
33. Babu, P. K.; Oldfield, E.; Wieckowski, A. In *Modern Aspects of Electrochemistry*; Vayenas, C. G.; Conway, B. E.; White, R. E., Eds.; Kluwer Academic/Plenum Publishers: New York, 2003; Vol. 36, Ch. 1.
34. Rice, C.; Tong, Y.; Oldfield, E.; Wieckowski, A. *Elecrochim. Acta* **1998**, *43*, 2825.
35. Ross, Jr., P. N. In *Electrocatalysis*; Lipkowski, J.; Ross, P. N., Eds.; Wiley-VCH: New York, 1988; Ch. 2.
36. Tong, Y.; Rice, C.; Wieckowski, A.; Oldfield, E. *J. Am. Chem. Soc.* **2000**, *122*, 1123.
37. Tong, Y. Y. *J. Magn. Reson. A* **1996**, *119*, 22.
38. Min, M. K.; Cho, J.; Cho, K.; Kim, H. *Electrochim. Acta* **2000**, *45*, 4211.
39. Tong, Y.; Rice, C.; Godbout, N.; Wieckowski, A.; Oldfield, E. *J. Am. Chem. Soc.* **1999**, *121*, 2996.
40. Park, S.; Xie, Y.; Weaver, M. J. *Langmuir* **2002**, *18*, 5792.
41. Park, S.; Tong, Y. Y.; Wieckowski, A.; Weaver, M. J. *Langmuir* **2002**, *18*, 3233.
42. Lu, C.; Rice, C.; Masel, R. I.; Babu, P. K.; Waszczuk, P.; Kim, H. S.; Oldfield, E.; Wieckowski, A. *J. Phys. Chem. B* **2002**, *106*, 9581.
43. Rudaz, S. L. *Ph.D. Thesis*, University of Illinois at Urbana-Champaign: 1984.